ACS Sustainable Chemistry & Engineering

pubs.acs.org/journal/ascecg

Research Article

Facile Synthesis and Integration of Poly(vinyl alcohol) Sponge-Supported Metal Nanocatalysts on a Microfluidic Chip Enable a New Continuous Flow Multireactor Nanocatalysis Platform for High Efficiency and Reusability Catalysis

Kaiqiang Hu, Lei Ma, Zonghua Wang,* Olivia Fernandez-Delgado, Yahir E. Garay, Jorge A. Lopez, and XiuJun Li*

Cite This: *ACS Sustainable Chem. Eng.* 2022, 10, 10579−10589

Read Online

ACCESS | Metrics & More | Article Recommendations | Supporting Information

ABSTRACT: A new poly(vinyl alcohol) (PVA) sponge-supported nanocatalysis platform on a continuous-flow microfluidic multireactor device was constructed for high-efficiency and high-reusability catalytic degradation of environmental pollutants. PVA sponge-supported metal nanoparticle catalysts (MNPs/PVA) were prepared by a simple improved impregnation self-assembly method, without any complicated surface modification. The MNPs/PVA catalysts were further integrated on a multireactor microfluidic device to form a continuous flow (CF) reactor platform (MNPs/PVA/chip) for simultaneous catalytic degradation of pollutants with two different nanocatalysts. After condition and catalyst optimizations, the catalytic activities of AuNPs/PVA and CoNPs/PVA were evaluated on this continuous flow microfluidic multireactor platform, by using *p*-nitrophenol (4-NP) as a model organic pollutant. Both catalysts exhibited outstanding catalytic efficiency (e.g., 100% for fresh catalysts), and the strong interactions between MNPs and PVA ensured high reusability (e.g., >20 cycles). After 20 cycles of catalysis, the optimal catalyst AuNPs/PVA still maintained a high catalytic efficiency of 97.6%. Compared to AuNPs/PVA-5, the cost-effective CoNPs/PVA catalyst exhibited similar catalytic performance within the first 10 cycles, while AuNPs/PVA showed better stability for long-term use. Hence, this continuous flow catalytic platform that combines the advantages of porous material-supported nanocatalysts with microfluidic devices has tremendous potential for various cost-effective environmental research and practical applications.

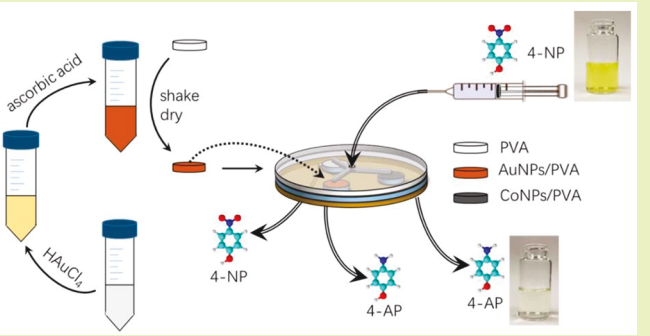

KEYWORDS: *Gold nanoparticles (AuNPs), Microfluidic devices, Continuous flow multireactor, Poly(vinyl alcohol) (PVA) sponge, Environmental catalysis, Nanocatalysts*

INTRODUCTION

Nitroaromatic compounds have been widely used as dyes, drugs, pesticides, herbicides, plasticizers, and explosives.[1] However, because of high toxicity and carcinogenesis and difficulties in their degradation, many nitroaromatic compounds such as *p*-nitrophenol (4-NP) in wastewater pose a serious threat to human health and the ecological environment,[2] though 4-NP is commonly used in industry as photographic developers, hair dyeing agents, and a potent intermediate in the synthesis of many analgesics and fever-reducing drugs.[3] Thus, the development of high-performance catalytic platforms for efficient and cost-effective degradation of 4-NP and other nitroaromatic compounds has become a hot topic in recent years.[4] Currently, most catalysts used for the 4-NP catalytic reduction are precious metals such as Au.[5] These noble metals have high catalytic efficiencies, but the cost is high. For example, various nanomaterials such as Au/TiO_2, Au colloidal solutions, and Pd-8 nanoclusters exhibited remarkable catalytic performances in 4-NP reduction but were difficult to recover, resulting in low reusability.[3,6] In contrast, some other catalysts exhibited high reusability with simple operations, but their catalytic efficiencies were not very high.[7,8] For instance, Song et al. reported an AgNPs catalyst encapsulated in hydrogels that needed 30 min to degrade 4-NP,[7] while Pan et al. reported a Ni/SBA-15 (0.1 wt%) catalyst that required 18 min to degrade 4-NP.[9] Therefore, there is a need for new cost-

Received: April 6, 2022
Revised: July 19, 2022
Published: July 29, 2022

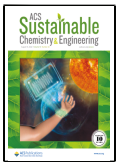

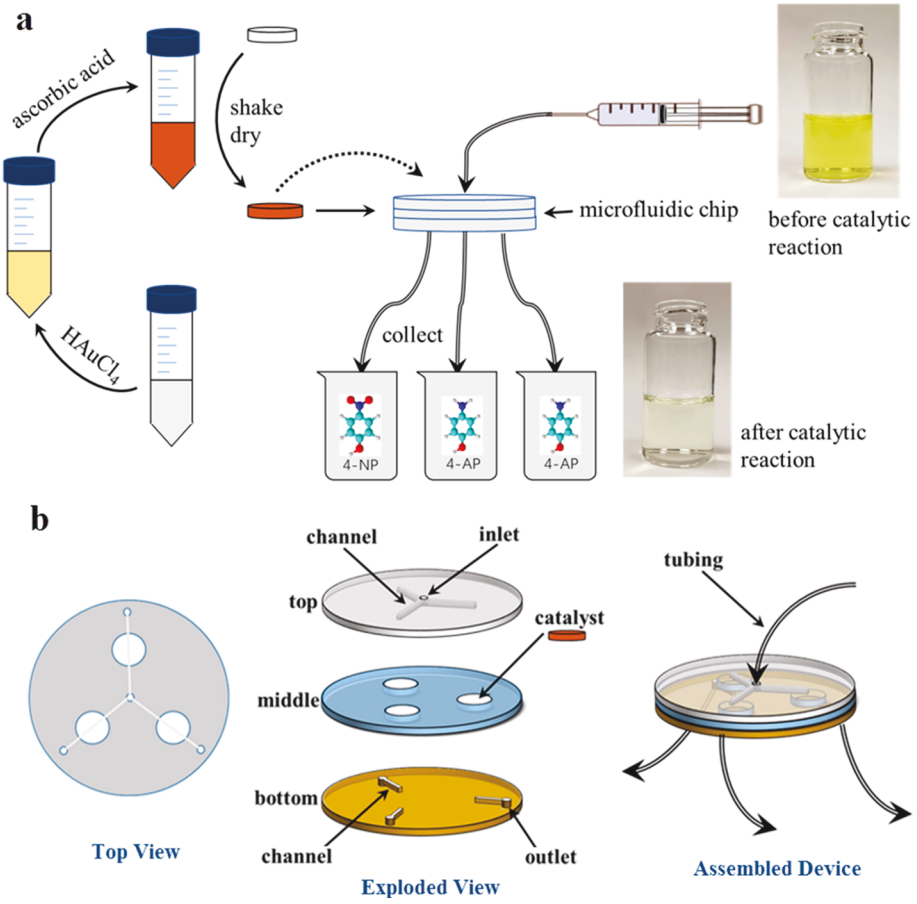

Figure 1. (a) Preparation and workflow of the AuNPs+CoNPs/PVA/chip microreactor platform. (b) Schematic of the microfluidic multireactor CF platform. The whole chip was composed of three layers. The circular multireactors in the middle layer were designed to support different loads of PVA-supported nanocatalysts.

effective and high-efficiency nanocatalytic systems but without compromised reusability.

Continuous flow (CF) is an important technique for catalysis,[6] green chemical synthesis,[10] medical,[11] and photothermal applications,[12] because of its high degree of automation, its ease of reaction control, the ability for scale-up reactions, and better reaction reproducibility.[13] These advantages guarantee that CF forms a superior technology for catalysis, compared to traditional batch reactors that face limitations of low efficiency, concentration gradient issues, and poor heat transfer.[14] Interestingly, accurate control of continuous flow is one important advantage of the recent microfluidic technology, which offers a unique opportunity for various fields from biomedical applications to nanomaterial catalysis.[15−19] It allows for fast analysis, high portability, and integrated processing and analysis of complex fluids with high efficiency and sensitivity.[16−18,20,21] Along with accurate control of flow,[22] the microfluidic technology can readily create multiple different microreactors and parallel channels for complex and well-controlled reactions and nanomaterial synthesis.[17,19,21,23] Furthermore, the customized multiple microreactors allow the integration of multiple different catalysts on a single platform, superior to conventional syringe-based CF systems.

Catalyst carriers such as TiO_2, hydrogel, and inorganic/organic polymers are usually integral components in continuous flow systems.[13] Catalyst carriers provide not only a strategy to immobilize catalysts for multiple instances of usage but also enable uniform distributions of nanocatalysts in porous materials of catalyst carriers, which offers another solution to ensure both high efficiency and reusability of nanocatalysts. A poly(vinyl alcohol) (PVA) sponge that is inexpensive, commercially available, and widely used in our daily life is a 3D high-porosity material with excellent chemical inertness and stability and, thus, has great potential as a cost-effective catalyst carrier. Additionally, the PVA sponge is rich in hydroxyl groups on the branched chains,[24] setting a solid framework to immobilize metal nanoparticles via strong interactions between hydroxyl groups with metal nanoparticles. But this commonly used inexpensive sponge, the PVA sponge, was rarely used as a catalyst carrier to link metal nanocatalysts. Thus, new low-cost, facile, and green catalytic strategies with high efficiency and reusability were highly desirable.[25]

The combination of porous material supported-metal nanocatalysts with a microfluidic device constitutes a remarkable continuous flow reactor platform. Herein, we report a new microfluidic CF platform integrated with multiple PVA-supported metal nanocatalysts for catalytic degradation of environmental pollutants with high efficiency and reusability. Two different kinds of metal nanoparticles (AuNPs and CoNPs) were prepared on the PVA sponge by an improved impregnation method to form the MNPs/PVA catalyst without any surface modification, and then the catalyst assembly was loaded on the multichannel microfluidic chip, forming an AuNPs/PVA/chip and CoNPs/PVA/chip multireactor continuous flow reactor platform. The microfluidic multireactor

https://doi.org/10.1021/acssuschemeng.2c02060
ACS Sustainable Chem. Eng. 2022, 10, 10579−10589

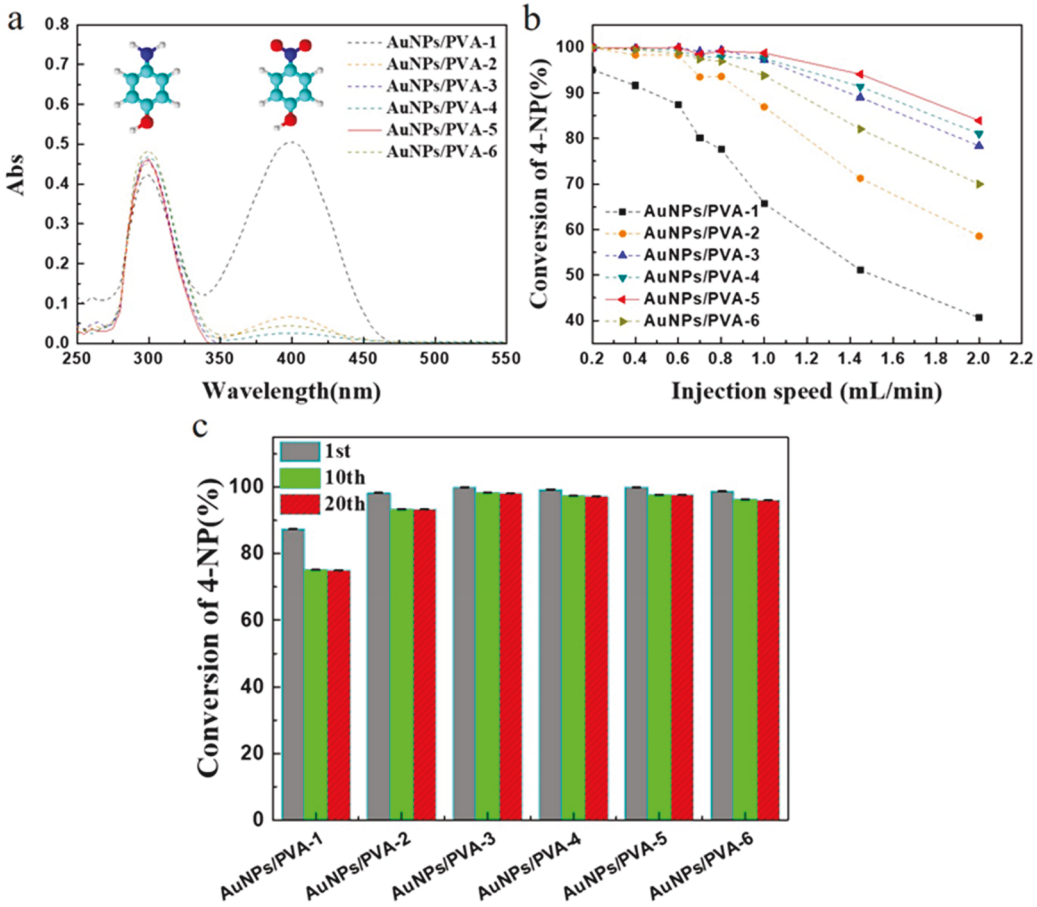

Figure 2. Catalytic efficiency of AuNPs/PVA catalysts in 4-NP degradation on the microfluidic CF platform using different catalyst groups (a) and at different injection speeds (b). (a) UV−vis spectra of 4-NP catalyzed by different AuNPs/PVA-(1−6) at 0.6 mL/min, (b) Conversion of 4-NP catalyzed by different AuNPs/PVA-(1−6) at different injection speeds. (c) Reusability studies by testing different 4-NP conversion rates of AuNPs/PVA-(1−6) at different catalysis cycles on the microfluidic CF platform. The injection speed was 0.6 mL/min.

CF platform allowed us to evaluate and compare the performance of these two different metal nanocatalysts simultaneously. We selected the 4-NP reduction in wastewater treatment as a model reaction to examine the catalytic performance of the catalysis platform. The preparation of the catalyst and the operation method of the catalytic process were simple, without the assistance of any bulky and costly instrumentation or complex catalytic procedures. The recovery of this spongy catalyst is facile, without the need for centrifugation. By utilizing this model, the MNPs/PVA/chip continuous flow reactor platform exhibited high catalytic efficiency and reusability. After 20 cycles of catalysis, the optimal group AuNPs/PVA still maintained a high catalytic efficiency of 97.6% in catalyzing 4-NP.

EXPERIMENTAL SECTION

Preparation and Workflow of the MNPs/PVA/Chip Microreactor Platform. The schematic in Figure 1a presents the preparation and workflow of the AuNPs/PVA/chip reactor platform. First, the PVA sponge was cut into different circular disks (diameter: 11 mm; thickness: 2 mm) by a laser cutter. Second, 20 mL of ultrapure water was added to a 50 mL conical centrifuge tube to make a clear yellow $HAuCl_4$ (200 mM) solution, after stirring with a vortex mixer for 30 s. Then, an appropriate amount of ascorbic acid (1.8 M) was added to the $HAuCl_4$ solution, and the solution was kept stirring for 70 s by the vortex mixer to form a gold colloid solution. Afterward, four pieces of PVA sponge were placed in the gold colloid solution, and AuNPs would self-assemble on the surface of the PVA sponge on an orbital shaker at 220 rpm for 12 h. Third, the self-assembled AuNPs/PVA was taken out, washed with ultrapure water, and then dried to obtain the ready-to-use AuNPs/PVA catalyst. To obtain optimal catalysts, different groups of metal nanocatalysts were prepared by varying the total amounts of the metal precursor while keeping the same ratio between the metal precursors and the corresponding reducing agents. Detailed information about the preparation of different groups of AuNPs/PVA and CoNPs/PVA is listed in Tables S1 and S2, respectively. Finally, the prepared AuNPs/PVA catalyst was loaded onto a microfluidic chip (Figure 1b), as described in the SI, forming the AuNPs/PVA/chip continuous flow reactor platform. Following a similar procedure, we prepared CoNPs/PVA and loaded it on the chip, except that the metal precursor for AuNPs and ascorbic acid were substituted by $Co(NO_3)_2$ and by $NaBH_4$, respectively.

Design and Fabrication of Microfluidic CF Microreactors. As shown in Figure 1b, three separate units with corresponding microreactors and channels were designed on the microfluidic CF platform for AuNPs/PVA, CoNPs/PVA, and the negative control, respectively, following our previously reported fabrication procedures using a laser cutter (Zing 16-30w, Epilog, America).[18] The exploded view in Figure 1b shows that the microfluidic chip consisted of three layers: the top layer had a central reservoir as a common inlet, with channels engraved on the inner surface; the middle layer had three circular microwells to load MNPs/PVA catalysts, while multiple channels on the upper side of the bottom layer were fabricated to collect the solutions after the catalytic reactions. Figure S1a shows

https://doi.org/10.1021/acssuschemeng.2c02060
ACS Sustainable Chem. Eng. 2022, 10, 10579−10589

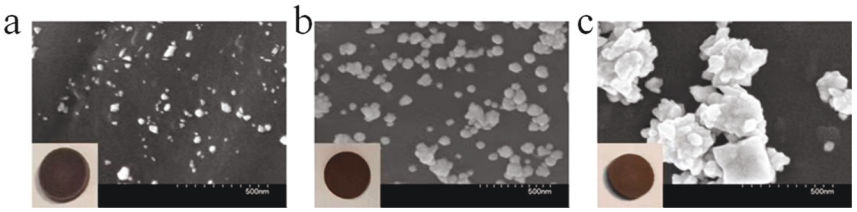

Figure 3. SEM images of different catalysts: (a) AuNPs/PVA-1, (b) AuNPs/PVA-5, and (c) AuNPs/PVA-6. The insets were photographs of the prepared catalysts with slightly different colors.

more specifics of the chip design, while Figure S1b shows photographs of these three different layers after fabrication.

RESULTS AND DISCUSSION

Catalytic Efficiency and Reusability of AuNPs/PVA on the Microfluidic CF Platform. *Catalytic Efficiency of AuNPs Catalysts in Microfluidic CF Reactions under Different Conditions.* UV−vis spectra were used to characterize the 4-NP catalytic reduction. As shown in Figure S2, the yellow mixture of $NaBH_4$ and 4-NP had a maximum characteristic absorbance peak at 400 nm for 4-NP before the catalytic reaction because of the formation of 4-nitrophenol ions. After the catalytic reaction, the solution became colorless (see the insets in Figure 1a), and the absorbance peak shifted from 400 to 300 nm, which was consistent with previous literature reports.[26] Hence, the absorbance changes at 400 nm were used to monitor the 4-NP degradation reaction. On the other hand, because of the color changes of the solution during the reaction process, the concentration of the remaining 4-NP can also be evaluated semiquantitatively by the color depth of the solution. The darker the color, the higher the concentration, and the lower the conversion rate.

Because the amount of the catalyst can significantly affect the catalysis, the catalytic efficiencies of different groups of catalysts for the 4-NP reduction under the same injection speed were studied for the optimal group of catalysts. We prepared six groups of catalysts (AuNPs/PVA-(1−6)) by varying the total amounts of AuNPs to be synthesized (see Table S1). Figure 2a shows the UV−vis spectra of AuNPs/PVA-(1−6) catalyzed 4-NP reactions when the injection speed was 0.6 mL/min. It can be seen that the absorption peak intensities at 400 nm varied significantly, indicating different catalytic efficiencies from different groups of AuNPs/PVA catalysts. When AuNPs/PVA-5 was used as the catalyst, the absorption peak intensity at 400 nm became 0, indicating a complete degradation of 4-NP to *p*-aminophenol (4-AP), that is, the catalytic efficiency for 4-NP was 100%. Therefore, AuNPs/PVA-5 (Au precursor concentration 3.0 mM) was determined as the best catalyst among the six groups of synthesized catalysts.

According to Table S1, the Au precursor concentration increased from 0.5 mM in AuNPs/PVA-1 to 4.0 mM in AuNPs/PVA-6, which usually led to a higher amount of metal nanocatalysts. Thus, it was not hard to understand how the catalytic efficiency increased from AuNPs/PVA-1 to AuNPs/PVA-5. However, AuNPs/PVA-6 did not exhibit a better catalytic efficiency than AuNPs/PVA-5. Instead, its catalytic efficiency was significantly lower than that of AuNPs/PVA-5 at higher injection speeds (Figure 2b), indicating some other factors affecting the catalytic efficiency such as the size and structure of metal nanoparticles. Therefore, the morphologies of these six prepared groups of catalysts were characterized by scanning electron microscopy (SEM). Figure 3 displays three representative SEM images from AuNPs/PVA-1, AuNPs/PVA-5, and AuNPs/PVA-6. The particle size distribution of AuNPs/PVA-1 and AuNPs/PVA-5 was more uniform, and no apparent aggregation was observed, compared to AuNPs/PVA-6. The particle sizes of AuNPs/PVA-1 and AuNPs/PVA-5 were approximately 50 and 200 nm, respectively, leading to a larger specific surface area of these nanoparticles, when compared to AuNPs/PVA-6. Although AuNPs-1 particles were smaller than those of AuNPs-5, the total amount of $HAuCl_4$ used in the AuNPs/PVA-1 synthesis was sixfold less than that used in AuNPs/PVA-5, resulting in a lower catalytic efficiency from AuNPs/PVA-1 than from AuNPs/PVA-5. However, notable aggregation was observed in AuNPs/PVA-6. The particle size in AuNPs/PVA-6 varied significantly in a range from 200 to 500 nm, which was not as uniform as other catalysts. The aggregated large nanoparticles were the main reason that caused lower catalytic efficiency of AuNPs/PVA-6 than AuNPs/PVA-5, which was consistent with previous literature reports.[27]

During continuous-flow reactions, the injection speed is another important factor affecting the catalytic efficiency. Especially when the speed is too fast, the pollutant may flow too fast to react with the catalyst. Hence, the effect of the injection speed on catalytic performance was studied as well. The conversion rates of AuNPs/PVA-(1−6) catalyzed 4-NP at different injection speeds (0.2 to 2 mL/min) are shown in Figure 2b. Overall, the conversion of 4-NP decreased with the increase of the injection speed. When the injection speed was lower than 0.6 mL/min, except for AuNPs/PVA-1, the conversion of 4-NP in all other groups was close to 100%. This indicates that most of the prepared catalysts had good catalytic performance for 4-NP degradation. However, when the injection speed reached above 0.6 mL/min, a significant decrease in the conversion was observed in most groups, especially for AuNPs/PVA-1, AuNPs/PVA-2, and AuNPs/PVA-6. When the injection speed was 2 mL/min, each group had the largest difference in catalytic efficiency, and the conversation rates of AuNPs/PVA-1, AuNPs/PVA-2, and AuNPs/PVA-6 decreased to 40.7%, 58.6%, and 70.0%, respectively. This was because as the injection speed increased, which reduced the contact time with AuNPs,[28] the effective collision frequency of activated molecules on the surface of the AuNPs decreased. Therefore, considering both the reaction throughput and the catalytic efficiency, 0.6 mL/min was selected as the optimal injection speed.

When comparing different catalyst groups at the same injection speed, AuNPs/PVA-5 had the strongest catalytic ability. Figure S4 showed the UV−vis spectra of 4-NP catalyzed by AuNPs/PVA-5 in a range of injection speeds from 0.2 to 2.0 mL/min. As the injection speed decreased, the absorption peak intensity at 400 nm gradually decreased, and

https://doi.org/10.1021/acssuschemeng.2c02060
ACS Sustainable Chem. Eng. 2022, 10, 10579−10589

when the injection speed reached 0.6 mL/min, the peak intensity became 0. The 4-NP conversion rates were 100% when the injection speed was slower than 0.6 mL/min (Figure 2b); when increasing the injection speed to 1.0 mL/min, the conversion rate could still reach 98.8%. In summary, the catalytic ability of AuNPs/PVA-5 to 4-NP increased with the decrease of the injection speed, and the maximum catalytic efficiency was achieved when the injection speed was at or slower than 0.6 mL/min. This further confirmed that the selected AuNPs/PVA-5 was the best catalyst among the six catalyst groups. A total of 5 mL of 4-NP (2.50 μmol in total) was completely degraded to 4-AP within 8.3 min on the microfluidic CF platform at a conversion rate of 100%, which was better than the reported values from previous works of literature, as listed in Table 1. For instance, in contrast, it took 83.3 min to degrade 1.28 μmol of 4-NP with the catalyst of Cu-Ag-Au@β-LGF CMRs at the conversion rate of 89% from a previous report.[29] Electrospinning fibers and aerogels were also reported as carriers to catalyze 4-NP by loading Au;[30−33] however, only a small amount of 4-NP (e.g., 0.122 μmol) was degraded, and the reaction times (e.g., 60 min) in these studies were longer than our time. Taken together, considering the catalytic efficiency, reaction time, and catalytic capacity, the AuNPs/PVA-5 catalyst has outstanding catalytic efficiency.

Table 1. Comparison of the Catalytic Efficiency and Reusability of the AuNPs/PVA/Chip with Reported Data[a]

catalyst	4-NP (μmol)	conversion (%)	time (min)	cycle times	ref
AuNPs/PVA	2.500	100	8.3 min	20	this work
Au/graphene hydrogel	0.280	100	12.0 min	-	5
Fe_3O_4@PBLG@AuNPs	0.500	100	50.0 min	9	34
graphene/PDA-AuNPs	1.000	100	13.0 min	3	35
Cu-Ag-Au@β-LGF CMRs	1.280	89	83.3 min	8	29
AuNP@electrospun PAN nanofibers	0.122	≈100	60.0 min	-	30
AuNPs@PAN/BTA1	0.150	100	90.0 min	4	31
Au@polymer@fiber nanocomposite	0.025	100	10.0 min	9	32
rGO/Au nanoparticle aerogel	2.500	100	18.0 min	5	33

[a]PAN: polyacrylonitrile. BTA1: benzene-1,3,5-tricarboxamide.

Reusability of AuNPs Catalysts in Microfluidic CF Reactions. Reusability is another important factor in evaluating the stability and performance of solid-phase catalysts. We studied the reusability of six groups of AuNPs/PVA/chip catalysts by studying their catalytic reduction of 4-NP from the 1st to the 20th cycles. Figure 2c shows the catalytic results of 4-NP catalyzed by AuNPs/PVA/chip at the 1st, 10th, and 20th cycles, when the injection speed was 0.6 mL/min. Except for AuNPs/PVA-1, all other groups of catalysts exhibited high catalytic performance even after 20 cycles. For example, when AuNPs/PVA-5 was used as the catalyst, the conversion of 4-NP was still as high as 97.7% and 97.6% after 10 and 20 catalytic cycles, respectively. During these 20 cycles, 25 μmol of 4-NP were degraded by the same catalyst, indicating outstanding reusability of our CF catalytic platform, whereas other catalysts listed in Table 1 could only sustain 1 to 9 cycles and degrade less 4-NP (e.g., 0.28 or 0.50 μmol) but with longer reaction times (e.g., 83.3 or 90 min). Similarly, there were minor differences observed between Cycle 1 and Cycle 10, and almost no changes were observed between Cycle 10 and Cycle 20 for other catalysts from AuNPs/PVA-2 to AuNPs/PVA-6, indicating stable catalysts, strong binding between AuNPs and the carrier PVA, and thus high reusability. This was attributed to the abundance of −OH functional groups on the PVA surface to form strong interactions with AuNPs, whichwas similar to the interactions between the paper pulp and the gold nanosponge that we reported previously.[26]

Catalytic Ability and Reusability of CoNPs/PVA/Chip. Considering that most catalysts used for the 4-NP catalytic reduction are precious metals such as Au and Ag,[5] to develop cost-effective catalysts for the degradation of aromatic pollutants, we prepared and tested the performance of the PVA sponge-supported CoNPs (CoNPs/PVA) catalyst for the catalytic degradation of 4-NP on the microfluidic CF platform, as cobalt is a nonprecious metal. We prepared five groups of catalysts (CoNPs/PVA-(1−5)) by varying the amounts of $Co(NO_3)_2$ solutions during the CoNPs synthesis process. Because we tested the performance of CoNPs/PVA and AuNPs/PVA on the same microfluidic platform, the injection speed in the experiment was the same as that of the AuNPs/PVA. Figure 4a showed the UV−vis spectra of catalytic reduction of 4-NP by CoNPs/PVA-(1−5). When the injection speed was 0.6 mL/min, the absorption peak intensity of 4-NP catalyzed by CoNPs/PVA-4 at 400 nm was the smallest, indicating the highest catalytic efficiency from CoNPs/PVA-4. Figure 4b shows the conversion rates from these five groups of catalysts, in which CoNPs/PVA-1 had the lowest conversion (81.8%), while other catalysts exhibited similar but higher catalytic performance. Given the highest conversion rate of 99.6% from CoNPs/PVA-4, CoNPs/PVA-4 was used as the optimal catalyst among these five groups of prepared catalysts.

Additionally, we studied the reusability of these five groups of CoNPs/PVA catalysts. The catalytic results of 4-NP catalyzed by CoNPs/PVA at the 1st, 10th, and 20th times were shown in Figure 4b. Most catalysts had a high catalytic performance (around 99%), except CoNPs/PVA-1 after the 1st cycle (81.8%). However, with the increase in catalytic cycles, the catalytic performance of each group of CoNPs/PVA slightly decreased, which was probably because CoNPs are susceptible to oxidation, resulting in a drop in conversion rates. In this microfluidic CF platform, $NaBH_4$ was included in the reaction solution, which could reduce the oxidation of CoNPs as a result of the reducing ability of $NaBH_4$, enabling CoNPs/PVA to maintain the maximum catalytic ability. Slight CoNPs loss could be another factor, as discussed in the following sections. Compared with other CoNPs/PVA groups, after 10 cycles and 20 cycles of catalysis, the conversion rates of 4-NP catalyzed by CoNPs/PVA-4 were still as high as 97.5% and 95.1%, respectively, exhibiting excellent reusability of the CoNPs/PVA-4 catalysts.

The morphologies of PVA and CoNPs/PVA-4 were characterized by SEM. The SEM image of PVA (Figure 4d) shows that PVA had a three-dimensional mesh structure, providing a high capacity to load nanoparticle catalysts as a carrier. A higher resolution SEM image in Figure 4c shows that CoNPs-4 were attached to the PVA framework with a particle size of about 400 nm. Those CoNPs could maintain 20 times of catalysis at high catalytic efficiency (>95.1% conversion rate at Cycle 20), indicating fairly strong binding between CoNPs

https://doi.org/10.1021/acssuschemeng.2c02060
ACS Sustainable Chem. Eng. 2022, 10, 10579−10589

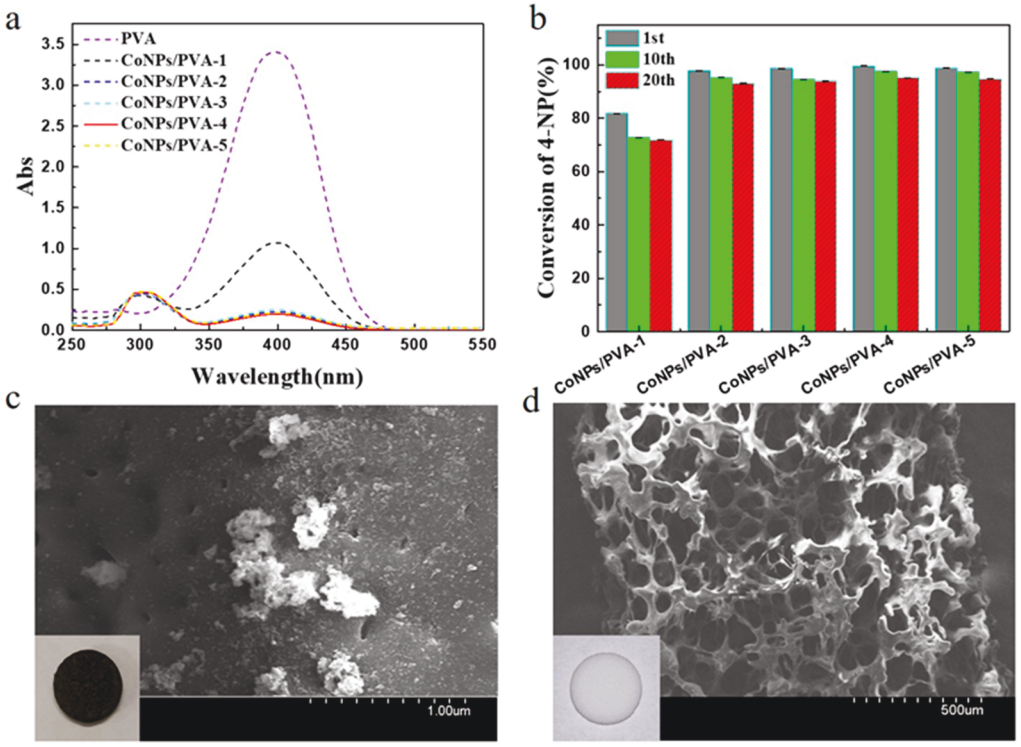

Figure 4. Investigation of the catalytic ability and reusability of CoNPs/PVA on the microfluidic CF platform. (a) UV−vis spectra of 4-NP reduction catalyzed by different new CoNPs/PVA-(1−5) catalysts at 0.6 mL/min. (b) Conversion of 4-NP catalyzed by different CoNPs/PVA-(1−5) catalysts after different catalytic cycles at 0.6 mL/min. (c, d) SEM images of CoNPs/PVA-4 and PVA.

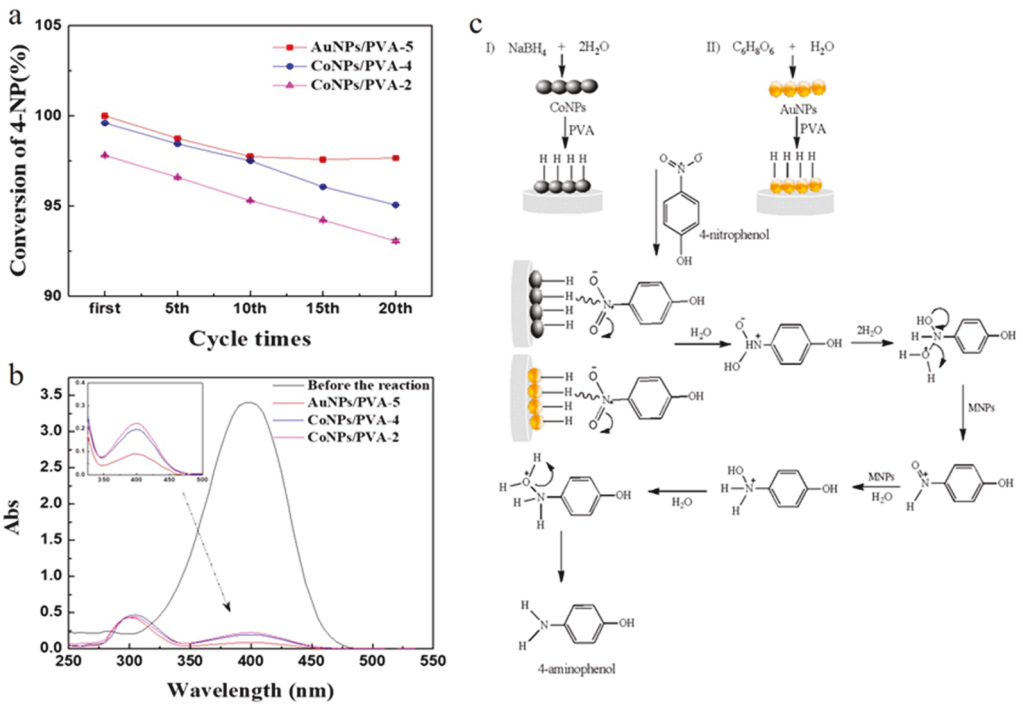

Figure 5. Comparison of the catalytic capabilities among AuNPs/PVA-5, CoNPs/PVA-4, and CoNPs/PVA-2. (a) Conversion changes by AuNPs/PVA-5, CoNPs/PVA-4, and CoNPs/PVA-2 over catalysis cycles. (b) UV−vis spectra of 4-NP catalyzed by AuNPs/PVA-5, CoNPs/PVA-4, and CoNPs/PVA-2. (c) Mechanism of catalytic reduction of 4-NP by AuNPs/PVA and CoNPs/PVA.

and PVA. Additionally, the well-distributed pores allowed the reaction solution to fully contact with the catalyst to achieve high catalytic efficiency. When compared with other catalysts listed in Table 1, CoNPs/PVA-4 exhibited not only high catalytic efficiency (e.g., 99.6%) but also high reusability (e.g., 20 cycles of catalysis), while other catalysts only demonstrated less than 10 cycles of catalysis. Considering most existing catalysts are precious metal-based catalysts (Table 1), CoNPs/

https://doi.org/10.1021/acssuschemeng.2c02060
ACS Sustainable Chem. Eng. 2022, 10, 10579−10589

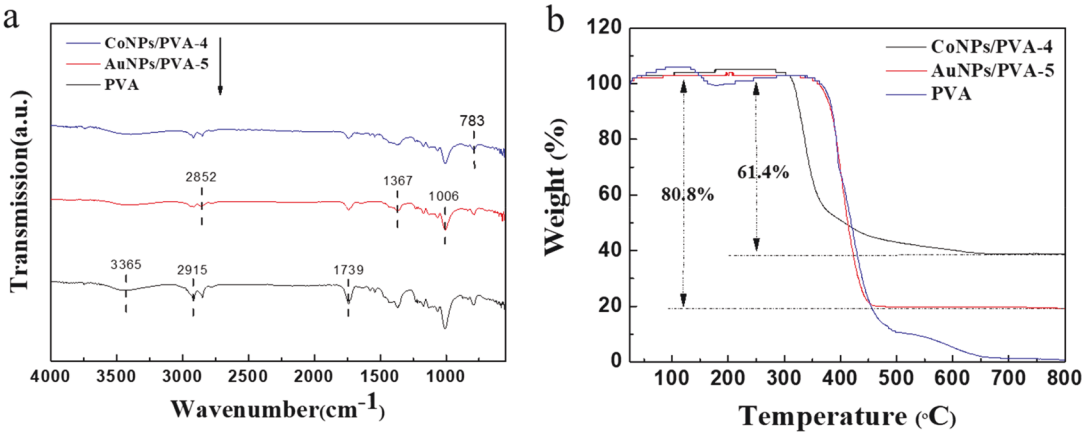

Figure 6. (a) FT-IR spectra of AuNPs/PVA-5, CoNPs/PVA-4, and PVA. (b) TGA thermograms of AuNPs/PVA-5, CoNPs/PVA-4, and PVA.

PVA may provide a new solution for cost-effective catalysis with high efficiency and reusability.

Comparison of the Catalytic Performance of AuNPs/PVA-5 and CoNPs/PVA-4 and Exploration of the Catalytic Mechanism. Leveraging the multiple parallel channels and microwells as multireactors, we achieved simultaneous 4-NP catalytic reductions on the same microfluidic continuous flow platform using two different catalysts, i.e., AuNPs/PVA-5 and CoNPs/PVA-4, as discussed earlier. This also allows us to evaluate the catalytic performance of different catalysts at the same time under the same experimental conditions on the same microfluidic CF platform.

We studied the difference in the conversions of 4-NP catalyzed by optimal groups of catalysts, AuNPs/PVA-5 and CoNPs/PVA-4, under different cycle times, as shown in Figure 5a and Figure S5. When being used for the first time, AuNPs/PVA-5 and CoNPs/PVA-4 had high conversions of 100% and 99.6%, respectively. As the number of repeated uses increased from 1 to 10, the catalytic abilities of both CoNPs/PVA and AuNPs/PVA decreased. When the number of catalysis cycles was 10, the conversion rates of 4-NP catalyzed by AuNPs/PVA-5 and CoNPs/PVA-4 were very similar, i.e., 97.7% and 97.5%, respectively. When the number of catalysis cycles was 20, the discrepancy between the conversions, which were 97.6% and 95.1% for AuNPs/PVA-5 and CoNPs/PVA-4, respectively, became greater. The catalytic ability of CoNPs/PVA-4 gradually kept decreasing after Cycle 10, which was probably related to the potential oxidation of CoNPs and the catalyst loss due to weaker binding between CoNPs with PVA, whereas the catalytic ability of AuNPs/PVA-5 was more stable and did not change much from Cycle 10 to Cycle 20, indicating stronger interaction between AuNPs and PVA, as shown in the following FT-IR, TGA, and XPS analyses. Similarly, the UV−vis spectra comparison at Cycle 20 in Figure 5b and the conversion difference between Cycle 1 and Cycle 20 from Figure S5 show that AuNPs/PVA-5 had better catalytic activities than CoNPs/PVA-4. In other words, under the same reaction conditions, the optimal catalyst AuNPs/PVA-5 exhibited better catalytic efficiency than CoNPs/PVA-4 after 10 catalysis cycles, implying higher reusability, though both exhibited similar catalytic efficiencies within the first 10 catalysis cycles. In comparison, the maximum cycle number from other reported catalysts in Table 1 was only 9.

Because the moles of metal in AuNPs/PVA-5 (0.015 mmol) and CoNPs/PVA-4 (0.030 mmol) were different, we further compared the catalytic performances of AuNPs/PVA-5 and CoNPs/PVA-2 (0.015 mmol), which had the same metal amounts (0.015 mmol). As shown in Figure 5a, CoNPs/PVA-2 had slightly lower conversion rates, which were 97.8%, 95.2%, and 93% after the first, tenth, and twentieth cycles, respectively, than those of both AuNPs/PVA-5 and CoNPs/PVA-4. A similar observation was found in the UV−vis spectra (Figure 5b). Although the catalytic performance of CoNPs/PVA-2 was slightly lower, it still exhibited impressive catalytic performance after 20 cycles, which was still superior to other reported catalysts listed in Table 1. For instance, graphene/PDA-AuNPs only demonstrated three catalysis cycles.

Super efficiency in both AuNPs and CoNPs catalyzed reactions is attributed to the close chemical and mechanical natures of these nanoparticles, which include high effective surface areas and efficient electron exchangeability to facilitate proton transfer, because hydrogen species are adsorbed on the metal nanoparticle surface, instead of being covalently bonded to the metal surface as in chemical catalysts. Thus, their mechanism of action should be similar, as proposed in Figure 5c. In the presence of excess $NaBH_4$, BH_4^- would adsorb onto the catalyst surface and transfer active hydrogen species to the particle surface to form a metal hydride complex. In the case of ascorbic acid, the hydrogen transfer occurs between one of its hydroxyl groups at the far end. When 4-NP chemically interacts with the catalyst surface, metal nanoparticles would transfer accepted electrons from BH_4^- to 4-NP. As a result, the adsorbed hydrogen species would transfer to the nitro groups, inducing their reduction to amino groups, as shown in Figure 5c with more details. Although the proposed mechanism needs to be further verified (not the focus of this article), as can be from Figure 5c, metal nanoparticles play a crucial role in the degradation of 4-NP, which can be confirmed by the fact that, without the metal nanoparticle's catalysis, the color of 4-NP may not fade in several days. It was also reported that the transformation from 4-NP to 4-AP was thermodynamically favorable but kinetically unfavorable without the catalyst,[36] further confirming the crucial role of MNPs in the catalytic reaction mechanism.

When selecting catalysts in practical applications, various aspects such as catalytic ability and catalyst costs need to be systematically considered. The catalytic abilities and the catalyst costs of AuNPs/PVA-5, CoNPs/PVA-4, and CoNPs/PVA-2 are summarized in Table S3. In terms of catalytic ability, although the AuNPs/PVA catalyst exhibited

https://doi.org/10.1021/acssuschemeng.2c02060
ACS Sustainable Chem. Eng. 2022, 10, 10579−10589

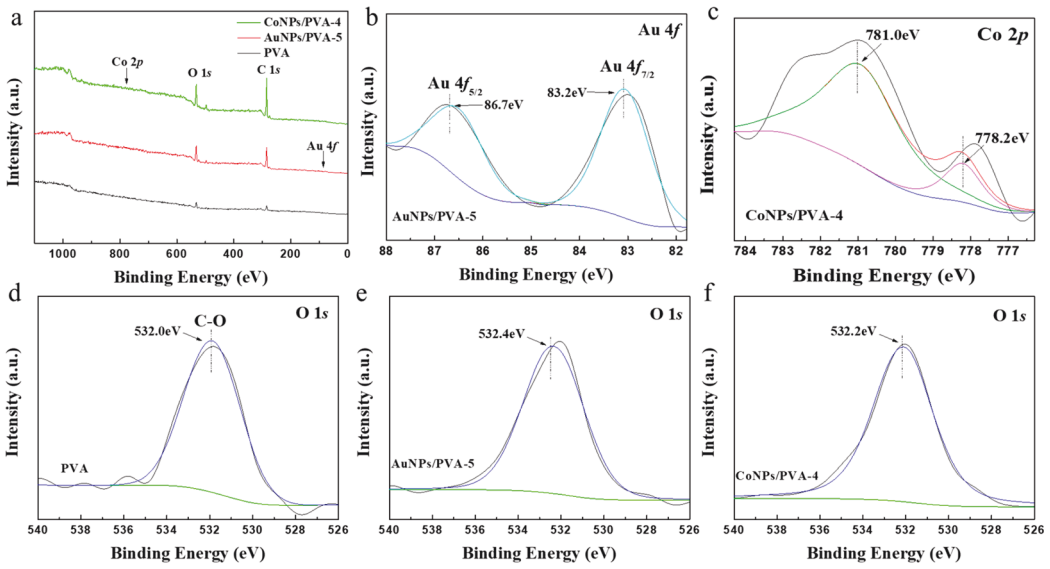

Figure 7. XPS characterization of PVA, AuNPs/PVA-5, and CoNPs/PVA-4. (a) Full survey. (b) Au 4*f* spectra of AuNPs/PVA-5. (c) Co 2*p* spectra of CoNPs/PVA-4. (d) O 1*s* spectra of PVA. (e) O 1*s* spectra of AuNPs/PVA-5. (f) O 1*s* spectra of CoNPs/PVA-4.

higher catalysis efficiency than the other two CoNPs/PVA catalysts, they all showed excellent catalytic efficiency (>93%) and reusability within 20 cycles. However, the cost of AuNPs/PVA-5 is 120 times and 250 times more expensive than that of CoNPs/PVA-4 and CoNPs/PVA-2, respectively. Thus, CoNPs/PVA may be a cost-effective catalyst for applications within 20 cycles. For higher than 20 cycles, AuNPs/PVA becomes a better choice. To show the activity of the platform, the conversion of another organic pollutant (*o*-nitroaniline (2-NA)) in the platform was tested. As shown in Figure S6, the platform also showed good catalytic ability for 2-NA.

Characterization Analysis. *FT-IR Analysis.* FT-IR was performed to characterize functional groups of PVA-supported catalysts and the carrier PVA, which also helped us understand possible interactions between the PVA matrix and the MNPs. The FT-IR spectra (550−4000 cm^{-1}) of PVA and MNPs/PVA were shown in Figure 6a. The results indicate that the FT-IR spectra of these samples were similar, with most peaks attributed to PVA. No major peak shift was observed, indicating that the original chemical PVA structure was not significantly changed during the process of PVA loading metal nanoparticles. As per the literature, the band at 3365 cm^{-1} was assigned to the stretching vibrations of O−H from PVA.[37] The bands at 2915 and 2852 cm^{-1} were attributed to the asymmetric stretching vibration of C−H. The prominent peak at 1739 cm^{-1} was due to the carbonyl group at the terminals of the polymer alcohol. The band at 1367 cm^{-1} was assigned to the vinyl C−H in-plane bending and H−C−H bending vibration. The band at 1006 cm^{-1} was attributed to the C−O−C stretching of the acetyl group present on the PVA. The band at 783 cm^{-1} was assigned to the stretching vibration of H−C−H. Figure 6a also shows that the peak intensity decreased slightly with the addition of MNPs, which was due to the decrease in the relative amount of PVA. The peak intensity at 3365 cm^{-1} decreased significantly after AuNPs were loaded, but the peak at 3365 cm^{-1} for CoNPs/PVA-4 did not decrease as much as that of AuNPs/PVA-5, indicating that AuNPs could consume more −OH during the MNPs growth process on PVA. This could alter some of the hydrogen bonding, leading to stronger binding between AuNPs and PVA than the interaction between CoNPs and PVA.

TGA Analysis. When preparing the catalytic reactor MNPs/PVA/chip, 120 °C was used to assemble the catalytic platform. Because catalysts are often used in a variety of complex reaction environments, we studied the thermal stability of catalysts by TGA analysis. Figure 6b showed the TGA thermograms of the PVA sponge and MNPs/PVA catalysts. We noticed that the first significant degradation phase of PVA was 130−175 °C (5.5% weight loss). However, AuNPs/PVA-5 and CoNPs/PVA-4 had no degradation phase in this temperature range. This weight loss of PVA was due to the evaporation of the bonded water from the polymer matrix.[38] The second degradation phase was 310−450 °C, which corresponded to the thermal degradation of PVA. The degradation temperature of CoNPs/PVA-4 was 310 °C, which was slightly lower than the degradation temperature of PVA. Because metals easily conducted heat, when the ambient temperature increased, Co conducted more heat to PVA, causing PVA to begin degradation at 310 °C. However, AuNPs/PVA-5 started to degrade at 325 °C, higher than the degradation temperature of CoNPs/PVA-4, indicating a stronger interaction between AuNPs and PVA than that of CoNPs and PVA, which was consistent with FT-IR analysis in supporting the higher reusability of AuNPs/PVA, as discussed in earlier sections. After TGA testing, the weight losses of CoNPs/PVA-4 and AuNPs/PVA-5 were calculated to be 61.4% and 80.8%, respectively, while the weight loss of the PVA sponge was almost 100%. Therefore, the amount of AuNPs in the PVA sponge could be inferred from the difference in weights. The content of AuNPs in AuNPs/PVA-5 was calculated to be 19.2%, and the content of CoNPs in CoNPs/PVA-4 was 38.6%.

XPS Analysis. The surface compositions and oxidation states of the catalysts are related to their catalytic performances, so XPS was applied to study the surface properties of the AuNPs/PVA-5 and CoNPs/PVA-4 catalysts. We performed the survey, C 1*s*, O 1*s*, Au 4*f*, and Co 2*p* XPS high-resolution scan spectra of PVA, AuNPs/PVA-5, and CoNPs/PVA-4 catalysts, as shown in Figure 7. It can be seen from Figure 7a that the

https://doi.org/10.1021/acssuschemeng.2c02060
ACS Sustainable Chem. Eng. 2022, 10, 10579−10589

PVA as a carrier was mainly composed of C and O elements. For the AuNPs/PVA-5 catalyst, as shown in Figure 7b, the strong doublets at 86.7 and 83.2 eV in Au 4*f* XPS spectra were attributed to Au^0 $4f_{5/2}$ and Au^0 $4f_{7/2}$, respectively. The binding energy (BE) of the Au $4f_{7/2}$ peak was used to evaluate the oxidation state of Au, which confirmed the good dispersion and metal form of gold (Au^0), indicating that Au^{3+} ions were completely reduced to Au^0 during the preparation of the catalyst.[39] As to the CoNPs/PVA-4 catalyst, as shown in Figure 7c, Co 2*p* XPS spectra show a peak at 778.2 eV, referring to the metallic state of Co. The result suggested the successful preparation of CoNPs. However, one peak at 781.0 eV indicates the existence of oxidized Co. This implied partial oxidation of CoNPs in the process of preparation and characterization of CoNPs.[40] Figure 7d−f shows the O 1*s* XPS spectra of PVA, AuNPs/PVA-5, and CoNPs/PVA-4 catalysts. PVA, AuNPs/PVA-5, and CoNPs/PVA-4 catalysts were all composed of single wide peaks (C−O). When PVA was loaded with metal Au, the binding energy shifted toward higher binding energy (a 0.4 eV increase), and we speculated that this was due to the strong interaction between the Au and the O atoms. The strong interaction ensured that the AuNPs catalyst would not be washed off of PVA after use, which was verified by washing three times during the AuNPs/PVA preparation steps and confirmed by high catalysis efficiency even after 20 catalysis cycles. Similarly, we also observed the binding energy of O 1*s* in CoNPs/PVA shifted 0.2 eV to a higher energy level, with less BE shift than AuNPs/PVA-5, which can explain why the catalytic efficiency of CoNPs/PVA kept decreasing. In addition, the intensity of the C−O peak from the C 1*s* XPS spectra of AuNPs/PVA-5 (Figure S7a−c) decreased greater than that of CoNPs/PVA-4, further indicating consumption of more hydroxyl groups from AuNPs/PVA-5 than from CoNPs/PVA-4 and, thus, stronger interactions between AuNPs and PVA. However, even though the catalytic efficiency of CoNPs/PVA decreased, the CoNPs/PVA still exhibited excellent reusability; i.e., it still achieved an impressive 95.1% 4-NP conversion after 20 catalysis cycles, particularly given the cost-effectiveness advantage of CoNPs/PVA.

CONCLUSIONS

A new facile continuous flow microfluidic catalytic multireactor platform integrated with different PVA sponge-supported nanocatalysts, for the first time, has been developed for continuous catalytic degradation of organic pollutants with high efficiency and high reusability. As a result of strong interactions between MNPs with PVA, the synthesized nanoparticles could be easily anchored on PVA by a simple impregnation method without any complicated surface modification. Taking advantage of multiple parallel microreactors on the microfluidic platform, multiple different metal nanoparticle catalysts on PVA were loaded onto the same microfluidic platform (i.e., AuNPs/PVA/chip and CoNPs/PVA/chip) for simultaneous catalytic reduction of 4-NP. The comparison of their catalytic performance under the same conditions on the same chip indicated that AuNPs had stronger interactions with the PVA sponge, thus leading to relatively longer reusability when compared to CoNPs, while CoNPs/PVA provided a new solution for cost-effective catalysis with high efficiency. These advantages enable great potential for the microfluidic CF catalysis platform to be applied to various research fields ranging from environmental remediation and wastewater treatment to the fine chemical industry.

ASSOCIATED CONTENT

Supporting Information

The Supporting Information is available free of charge at https://pubs.acs.org/doi/10.1021/acssuschemeng.2c02060.

Detailed experimental section and UV−vis and XPS spectra characterization (PDF)

AUTHOR INFORMATION

Corresponding Authors

XiuJun Li − *Department of Chemistry and Biochemistry, Environmental Science and Engineering, Material Science & Engineering, and Border Biomedical Research Center, Forensic Science, University of Texas at El Paso, El Paso, Texas 79968, United States;* orcid.org/0000-0002-7954-0717; Email: xli4@utep.edu

Zonghua Wang − *College of Chemistry and Chemical Engineering, Shandong Sino-Japanese Center for Collaborative Research of Carbon Nanomaterials, Instrumental Analysis Center of Qingdao University, Qingdao University, Qingdao 266071, PR China;* orcid.org/0000-0002-9120-4089; Email: wangzonghua@qdu.edu.cn

Authors

Kaiqiang Hu − *College of Chemistry and Chemical Engineering, Shandong Sino-Japanese Center for Collaborative Research of Carbon Nanomaterials, Instrumental Analysis Center of Qingdao University, Qingdao University, Qingdao 266071, PR China; Department of Chemistry and Biochemistry, University of Texas at El Paso, El Paso, Texas 79968, United States*

Lei Ma − *Department of Chemistry and Biochemistry, University of Texas at El Paso, El Paso, Texas 79968, United States;* orcid.org/0000-0002-8555-5085

Olivia Fernandez-Delgado − *Department of Chemistry and Biochemistry, University of Texas at El Paso, El Paso, Texas 79968, United States;* orcid.org/0000-0002-6641-026X

Yahir E. Garay − *Department of Physics, University of Texas at El Paso, El Paso, Texas 79968, United States*

Jorge A. Lopez − *Department of Physics, University of Texas at El Paso, El Paso, Texas 79968, United States*

Complete contact information is available at: https://pubs.acs.org/10.1021/acssuschemeng.2c02060

Notes

The authors declare no competing financial interest.

ACKNOWLEDGMENTS

We would like to acknowledge the financial support of our research from the U.S. NSF (IIP 2122712, IIP2052347, IIP1953841, and DMR1827745), the National Institute of Allergy and Infectious Disease of the NIH (R21AI107415), DOT (CARTEEH), Cancer Prevention and Research Institute of Texas (CPRIT; RP210165), the University of Texas at El Paso (UTEP) for the IDR Program, the Philadelphia Foundation, and the Medical Center of the Americas Foundation. Previous financial support to our research from the National Institute of General Medical Sciences of the NIH (SC2GM105584), the NIH/NIMHD RCMI Pilot grant (5G12MD007593-22), the NIH BUILDing Scholar Summer

Sabbatical Award, NSF (DMR1205302), the University of Texas (UT) System for the STARS award, and the Multidisciplinary Research Award Program (MRAP) and the URI Program from UTEP is also greatly acknowledged. We are also thankful to Dr. Luis Echegoyen's group for the TGA measurement and Mr. Yohannes Getahun for the help in manuscript preparation. Z.W. and K.H. would like to thank the Taishan Scholar Program of Shandong Province (No. ts201511027) and First-Class Fellowship in Chemistry from Shandong Province, China, for the support.

REFERENCES

(1) Xiong, Z.; Zhang, H.; Zhang, W.; Lai, B.; Yao, G. Removal of nitrophenols and their derivatives by chemical redox: A review. *Chemical Engineering Journal* **2019**, *359*, 13−31.

(2) Kovacic, P.; Somanathan, R. Nitroaromatic compounds: Environmental toxicity, carcinogenicity, mutagenicity, therapy and mechanism. *Journal of Applied Toxicology* **2014**, *34* (8), 810−824.

(3) Basavegowda, N.; Mishra, K.; Lee, Y. R. Trimetallic FeAgPt alloy as a nanocatalyst for the reduction of 4-nitroaniline and decolorization of rhodamine B: A comparative study. *J. Alloys Compd.* **2017**, *701*, 456−464.

(4) (a) Jiang, S.; Ling, L.; Xu, Z.; Liu, W.; Jiang, H. Enhancing the Catalytic Activity and Stability of Noble Metal Nanoparticles by the Strong Interaction of Magnetic Biochar Support. *Ind. Eng. Chem. Res.* **2018**, *57* (39), 13055−13064. (b) Gangula, A.; Podila, R.; M, R.; Karanam, L.; Janardhana, C.; Rao, A. M. Catalytic Reduction of 4-Nitrophenol using Biogenic Gold and Silver Nanoparticles Derived fromBreynia rhamnoides. *Langmuir* **2011**, *27* (24), 15268−15274. (c) Mehmood, S.; Janjua, N. K.; Saira, F.; Fenniri, H. AuCu@Pt Nanoalloys for Catalytic Application in Reduction of 4-Nitrophenol. *Journal of Spectroscopy* **2016**, *2016*, 1−8.

(5) Li, J.; Liu, C.-y.; Liu, Y. Au/graphene hydrogel: synthesis, characterization and its use for catalytic reduction of 4-nitrophenol. *J. Mater. Chem.* **2012**, *22* (17), 8426−8430.

(6) De Angelis, S.; Franco, M.; Triminì, A.; González, A.; Sainz, R.; Degennaro, L.; Romanazzi, G.; Carlucci, C.; Petrelli, V.; de la Esperanza, A.; et al. A Study of Graphene-Based Copper Catalysts: Copper(I) Nanoplatelets for Batch and Continuous-Flow Applications. *Chemistry-An Asian Journal* **2019**, *14* (17), 3011−3018.

(7) Song, J.; Zhu, Y.; Zhang, J.; Yang, J.; Du, Y.; Zheng, W.; Wen, C.; Zhang, Y.; Zhang, L. Encapsulation of AgNPs within Zwitterionic Hydrogels for Highly Efficient and Antifouling Catalysis in Biological Environments. *Langmuir* **2019**, *35* (5), 1563−1570.

(8) Li, J.; Wu, F.; Lin, L.; Guo, Y.; Liu, H.; Zhang, X. Flow fabrication of a highly efficient Pd/UiO-66-NH_2 film capillary microreactor for 4-nitrophenol reduction. *Chemical Engineering Journal* **2018**, *333*, 146−152.

(9) Pan, W.; Zhang, S.; He, F.; Gai, S.; Sun, Y.; Yang, P. A cheap and efficient catalyst with ultra-high activity for reduction of 4-nitrophenol. *CrystEngComm* **2015**, *17*, 5744−5750.

(10) Bennett, J. A.; Campbell, Z. S.; Abolhasani, M. Role of continuous flow processes in green manufacturing of pharmaceuticals and specialty chemicals. *Current Opinion in Chemical Engineering* **2019**, *26*, 9−19.

(11) Amerling, R.; Merouani, A. Continuous-Flow Peritoneal Dialysis as Acute Therapy. *Critical Care Nephrology* **2019**, 1128−1134.e1.

(12) Belekoukia, M.; Kalamaras, E.; Tan, J. Z. Y.; Vilela, F.; Garcia, S.; Maroto-Valer, M. M.; Xuan, J. Continuous flow-based laser-assisted plasmonic heating: A new approach for photothermal energy conversion and utilization. *Applied Energy* **2019**, *247*, 517−524.

(13) (a) Hone, C. A.; Lopatka, P.; Munday, R.; O'Kearney-McMullan, A.; Kappe, C. O. Continuous-flow Synthesis of Aryl Aldehydes by Pd-catalyzed Formylation of Aryl Bromides Using Carbon Monoxide and Hydrogen. *ChemSusChem* **2019**, *12* (1), 326−337. (b) Jin, Q.; Lu, B.; Pan, Y.; Tao, X.; Himmelhaver, C.; Shen, Y.; Gu, S.; Zeng, Y.; Li, X. Novel porous ceramic sheet supported metal reactors for continuous-flow catalysis. *Catal. Today* **2020**, *358*, 324−332.

(14) Jin, Q.; Shen, Y.; Li, X.; Zeng, Y. Resource utilization of waste deNO_x catalyst for continuous-flow catalysis by supported metal reactors. *Molecular Catalysis* **2020**, *480*, 110634.

(15) (a) Li, X. J.; Zhou, Y. *Microfluidic Devices for Biomedical Applications*; Woodhead Publishing (Elsevier): 2013. (b) Sibbitts, J.; Sellens, K. A.; Jia, S.; Klasner, S. A.; Culbertson, C. T. Cellular Analysis Using Microfluidics. *Anal. Chem.* **2018**, *90* (1), 65−85.

(16) (a) Zuo, P.; Li, X.; Dominguez, D. C.; Ye, B.-C. A PDMS/paper/glass hybrid microfluidic biochip integrated with aptamer-functionalized graphene oxide nano-biosensors for one-step multiplexed pathogen detection. *Lab Chip* **2013**, *13* (19), 3921−3928. (b) Li, X.; Dou, M.; Dominguez, D. C. Methods and compositions for paper-based and hybrid microfluidic devices integrated with nucleic acid amplification for disease diagnosis. U.S. Patent 10875024, 2020. (c) Sanjay, S. T.; Fu, G.; Dou, M.; Xu, F.; Liu, R.; Qi, H.; Li, X. Biomarker detection for disease diagnosis using cost-effective microfluidic platforms. *Analyst* **2015**, *140* (21), 7062−7081. (d) Dou, M.; Sanjay, S. T.; Dominguez, D. C.; Liu, P.; Xu, F.; Li, X. Multiplexed instrument-free meningitis diagnosis on a polymer/paper hybrid microfluidic biochip. *Biosens. Bioelectron.* **2017**, *87*, 865−873. (e) Dou, M.; Sanjay, S. T.; Benhabib, M.; Xu, F.; Li, X. Low-cost bioanalysis on paper-based and its hybrid microfluidic platforms. *Talanta* **2015**, *145*, 43−54. (f) Sanjay, S. T.; Zhou, W.; Dou, M.; Tavakoli, H.; Ma, L.; Xu, F.; Li, X. Recent advances of controlled drug delivery using microfluidic platforms. *Adv. Drug Delivery Rev.* **2018**, *128*, 3−28.

(17) Dou, M.; Garcia, J. M.; Zhan, S.; Li, X. Interfacial nano-biosensing in microfluidic droplets for high-sensitivity detection of low-solubility molecules. *Chem. Comm* **2016**, *52* (17), 3470−3473.

(18) (a) Sanjay, S. T.; Dou, M.; Sun, J.; Li, X. A paper/polymer hybrid microfluidic microplate for rapid quantitative detection of multiple disease biomarkers. *Sci. Rep.* **2016**, *6*, 30474. (b) Dou, M.; Sanjay, S. T.; Dominguez, D. C.; Zhan, S.; Li, X. A paper/polymer hybrid CD-like microfluidic SpinChip integrated with DNA-functionalized graphene oxide nanosensors for multiplex qLAMP detection. *Chem. Comm* **2017**, *53* (79), 10886−10889.

(19) Pekkari, A.; Say, Z.; Susarrey-Arce, A.; Langhammer, C.; Härelind, H.; Sebastian, V.; Moth-Poulsen, K. Continuous Microfluidic Synthesis of Pd Nanocubes and PdPt Core−Shell Nanoparticles and Their Catalysis of NO_2 Reduction. *ACS Appl. Mater. Interfaces* **2019**, *11* (39), 36196−36204.

(20) (a) Sanjay, S. T.; Fu, G.; Dou, M.; Xu, F.; Liu, R.; Qi, H.; Li, X. Biomarker detection for disease diagnosis using cost-effective microfluidic platforms. *Analyst* **2015**, *140* (21), 7062−7081. (b) Fu, G.; Zhu, Y.; Wang, W.; Zhou, M.; Li, X. Spatiotemporally Controlled Multiplexed Photothermal Microfluidic Pumping under Monitoring of On-Chip Thermal Imaging. *ACS Sensors* **2019**, *4* (9), 2481−2490. (c) Nyein, H. Y. Y.; Tai, L.-C.; Ngo, Q. P.; Chao, M.; Zhang, G. B.; Gao, W.; Bariya, M.; Bullock, J.; Kim, H.; Fahad, H. M.; et al. A Wearable Microfluidic Sensing Patch for Dynamic Sweat Secretion Analysis. *ACS Sensors* **2018**, *3* (5), 944−952. (d) Dou, M.; Macias, N.; Shen, F.; Dien Bard, J.; Domínguez, D. C.; Li, X. Rapid and Accurate Diagnosis of the Respiratory Disease Pertussis on a Point-of-Care Biochip. *EClinicalMedicine* **2019**, *8*, 72−77.

(21) (a) Fu, G.; Zhou, W.; Li, X. Remotely tunable microfluidic platform driven by nanomaterial-mediated on-demand photothermal pumping. *Lab Chip* **2020**, *20* (12), 2218−2227. (b) Wei, X.; Zhou, W.; Sanjay, S. T.; Zhang, J.; Jin, Q.; Xu, F.; Dominguez, D. C.; Li, X. Multiplexed Instrument-Free Bar-Chart SpinChip Integrated with Nanoparticle-Mediated Magnetic Aptasensors for Visual Quantitative Detection of Multiple Pathogens. *Anal. Chem.* **2018**, *90* (16), 9888−9896.

(22) (a) Shen, F.; Li, X.; Li, P. C. H. Study of flow behaviors on single-cell manipulation and shear stress reduction in microfluidic chips using computational fluid dynamics simulations. *Biomicrofluidics* **2014**, *8* (1), 014109. (b) Shen, F.; Li, Y.; Liu, Z.; Li, X. Study of flow

https://doi.org/10.1021/acssuschemeng.2c02060
ACS Sustainable Chem. Eng. 2022, 10, 10579−10589

behaviors of droplet merging and splitting in microchannels using Micro-PIV measurement. *Microfluid Nanofluid* **2017**, *21*, 66.
(23) Lv, M.; Zhou, W.; Tavakoli, H.; Bautista, C.; Xia, J.; Wang, Z.; Li, X. Aptamer-functionalized metal-organic frameworks (MOFs) for biosensing. *Biosens Bioelectron* **2021**, *176*, 112947.
(24) Luo, M.; Wang, W.; Zhao, Q.; Li, M.; Chen, Y.; Lu, Z.; Liu, K.; Wang, D. Chemiluminescence biosensor for hydrogen peroxide determination by immobilizing horseradish peroxidase onto PVA-*co*-PE nanofiber membrane. *Eur. Polym. J.* **2017**, *91*, 307−314.
(25) (a) Zhang, Z.; Cao, X.; Wang, G.; Zhang, G.; Zhang, X. Straightforward synthesis of biologically valuable nonsymmetrical malonamides under mild conditions. *Green Chem.* **2022**, *24*, 3035−3041. (b) Wan, Y.; Zhang, Z.; Ma, N.; Bi, J.; Zhang, G. Acylamino-Directed Specific Sequential Difunctionalizations of Anilides via Metal-Free Relay Reactions for p-Oxygen and o-Nitrogen Incorporation. *Journal of Organic Chemistry* **2019**, *84* (2), 780−791.
(26) Jin, Q.; Ma, L.; Zhou, W.; Shen, Y.; Fernandez-Delgado, O.; Li, X. Smart paper transformer: new insight for enhanced catalytic efficiency and reusability of noble metal nanocatalysts. *Chemical Science* **2020**, *11* (11), 2915−2925.
(27) Liu, F.; Liu, X.; Astruc, D.; Gu, H. Dendronized triazolyl-containing ferrocenyl polymers as stabilizers of gold nanoparticles for recyclable two-phase reduction of 4-nitrophenol. *J. Colloid Interface Sci.* **2019**, *533*, 161−170.
(28) Monteiro, R. A. R.; Silva, A. M. T.; Angelo, J. R. M.; Silva, G. V.; Mendes, A. M.; Boaventura, R. A. R.; Vilar, V. J. P. Photocatalytic oxidation of gaseous perchloroethylene over TiO_2 based paint. *J. Photochem. Photobiol., A* **2015**, *311*, 41−52.
(29) Huang, R.; Zhu, H.; Su, R.; Qi, W.; He, Z. Catalytic Membrane Reactor Immobilized with Alloy Nanoparticle-Loaded Protein Fibrils for Continuous Reduction of 4-Nitrophenol. *Environ. Sci. Technol.* **2016**, *50* (20), 11263−11273.
(30) Sawada, K.; Sakai, S.; Taya, M. Polyacrylonitrile-based electrospun nanofibers carrying gold nanoparticles in situ formed by photochemical assembly. *J. Mater. Sci.* **2014**, *49*, 4595−4600.
(31) Drummer, M.; Liang, C.; Kreger, K.; Rosenfeldt, S.; Greiner, A.; Schmidt, H.-W. Stable Mesoscale Nonwovens of Electrospun Polyacrylonitrile and Interpenetrating Supramolecular 1,3,5-Benzenetrisamide Fibers as Efficient Carriers for Gold Nanoparticles. *ACS Appl. Mater. Interfaces* **2021**, *13*, 34818−34828.
(32) Guarrotxena, N.; Garrido, L.; Quijada-Garrido, I. Design of Nanostructured Surfaces Based on Metal NP Precipitation Strategy and their Catalytic Application. *Advanced Materials Interfaces* **2018**, *5* (24), 1801374.
(33) Cao, X.; Yan, S.; Hu, F.; Wang, J.; Wan, Y.; Sun, B.; Xiao, Z. Reduced Graphene Oxide/Gold Nanoparticle Aerogel for Catalytic Reduction of 4-Nitrophenol. *RSC Adv.* **2016**, *6* (68), 64028−64038.
(34) Marcelo, G.; Muñoz-Bonilla, A.; Fernández-García, M. Magnetite-Polypeptide Hybrid Materials Decorated with Gold Nanoparticles: Study of Their Catalytic Activity in 4-Nitrophenol Reduction. *J. Phys. Chem. C* **2012**, *116* (46), 24717−24725.
(35) Luo, J.; Zhang, N.; Liu, R.; Liu, X. In situ green synthesis of Au nanoparticles onto polydopamine-functionalized graphene for catalytic reduction of nitrophenol. *RSC Adv.* **2014**, *4* (110), 64816−64824.
(36) Kamal, T.; Khan, S. B.; Asiri, A. M. Nickel nanoparticles-chitosan composite coated cellulose filter paper: An efficient and easily recoverable dip-catalyst for pollutants degradation. *Environ. Pollut.* **2016**, *218*, 625−633.
(37) (a) Mirzaee, S.; Shayesteh, S. F. Ultrasound induced strain in ultrasmall $CoFe_2O_4$@polyvinyl alcohol nanocomposites. *Ultrasonics Sonochemistry* **2018**, *40*, 583−586. (b) Rezaee, O.; Mahmoudi Chenari, H.; Ghodsi, F. E.; Ziyadi, H. Preparation of PVA nanofibers containing tungsten oxide nanoparticle by electrospinning and consideration of their structural properties and photocatalytic activity. *J. Alloys Compd.* **2017**, *690*, 864−872.
(38) Chowdhury, S.; Teoh, Y. L.; Ong, K. M.; Rafflisman Zaidi, N. S.; Mah, S.-K. Poly(vinyl) alcohol crosslinked composite packaging film containing gold nanoparticles on shelf life extension of banana. *Food Packaging and Shelf Life* **2020**, *24*, 100463.
(39) Cojocaru, B.; Neaţu, Ş.; Sacaliuc-Pârvulescu, E.; Lévy, F.; Pârvulescu, V. I.; Garcia, H. Influence of gold particle size on the photocatalytic activity for acetone oxidation of Au/TiO_2 catalysts prepared by dc-magnetron sputtering. *Applied Catalysis B: Environmental* **2011**, *107* (1−2), 140−149.
(40) Dong, W.; Zhuang, Y.; Li, S.; Zhang, X.; Chai, H.; Huang, Y. High peroxidase-like activity of metallic cobalt nanoparticles encapsulated in metal-organic frameworks derived carbon for biosensing. *Sens. Actuators, B* **2018**, *255*, 2050−2057.

https://doi.org/10.1021/acssuschemeng.2c02060
ACS Sustainable Chem. Eng. 2022, 10, 10579−10589